EES Batteries

PAPER

View Article Online
View Journal | View Issue

Cite this: *EES Batteries*, 2025, **1**, 511

Vanadium-encased zeolite based mixed matrix membrane for high-performance all-vanadium redox flow battery†

Chetan M. Pawar,[a,b] Rahulbhai Parmar,[b,c] Sooraj Sreenath,[a,b] Jayesh C. Chaudhari,[d] Govind Sethia *[b,c] and Rajaram K. Nagarale *[a,b]

Achieving high proton selectivity over vanadium ions is crucial for ensuring a long calendar life of vanadium redox flow batteries (VRFBs). Conventional perfluorinated and hydrocarbon-based membranes often struggle to prevent vanadium ion crossover, which compromises VRFB performance. This study highlights the modification of ZSM-5 (40) Na^+ zeolites with vanadium ions to leverage Donnan exclusion in a galvanostatic charge/discharge process. The membranes were prepared by physically blending the modified zeolite with sulfonated poly(ether ether ketone) (SPEEK). The developed membranes displayed excellent oxidative stability in 2 M H_2SO_4 containing 1.5 M VO_2^+ ions, along with enhanced electrochemical performance. In single-cell VRFB testing, the membrane with the highest proton conductivity, SPEEK-ZSM 40 VO_2^+, achieved an average coulombic efficiency of 98.0% and an energy efficiency of 80.37% over 200 continuous charge/discharge cycles at a current density of 80 mA cm^{-2}. Additionally, it demonstrated a capacity retention of 54% after 100 charge–discharge cycles. Furthermore, polarization curve analysis and self-discharge experiments demonstrated a peak power density of 330.45 mW cm^{-2} higher and a 1.3-fold slower self-discharge rate compared to the state-of-the-art Nafion-117® membrane under identical conditions. These findings emphasize the potential of zeolite-based mixed matrix membranes, utilizing Donnan exclusion, as a promising approach for enhancing the efficiency, durability, and operational stability of VRFBs.

Received 30th October 2024,
Accepted 28th March 2025

DOI: 10.1039/d4eb00023d

rsc.li/EESBatteries

Broader context

Large-scale deployment of redox flow batteries such as vanadium redox flow batteries (VRFBs) is a plausible solution to store and utilize intermittent renewable energy. Traditional separators in VRFBs are incapable of addressing the prominent inherent unmet issues *i.e.*, the vanadium ion permeability across the ion exchange membrane (IEM), resulting in capacity decay and reduced system efficiency. In recent years, the membrane research community has adopted different strategies to counter the cross-contamination of the vanadium ions and boost the overall performance of the battery. The benefit of Donnan exclusion has been considered by deployment of anion exchange membranes (AEMs) for VRFB. Unfortunately, AEMs have the limitation of low ionic conductivity and questionable chemical stability in highly oxidative flow battery environment. Mixed matrix membranes also emerge as an effective approach to develop high performance IEMs for VRFB. Herein, we report vanadium-encased ZSM-5 (40)-VO_2^+ zeolites into SPEEK polymer to obtain a mixed matrix membrane which leverages Donnan exclusion to profoundly reduce excess vanadium ion crossover, ensuring long-term operational stability. This unique strategy of infiltration of positive charge with the nanostructure followed by incorporation in a functionalized polymer matrix is a facile yet effective solution for developing ultra selective proton exchange membranes for VRFB applications.

1. Introduction

Vanadium redox flow batteries (VRFBs) are a promising technology for large-scale energy storage due to their inherent features, such as independent scalability of energy and power density, flexible architecture, and long lifespan.[1] Although VRFBs have been demonstrated at the commercial scale, the diffusion of vanadium ions across the two half-cells remains an unresolved issue.[2] To address this, different approaches have been adopted to develop new ion-exchange membranes.

[a]*Membrane Science and Separation Technology Division, Electro Membrane Processes Laboratory, CSIR-Central Salt and Marine Chemicals Research Institute, Bhavnagar 364002, India. E-mail: rknagarale@csmcri.res.in*
[b]*Academy of Scientific and Innovative Research (AcSIR), Ghaziabad – 201002, India*
[c]*Inorganic Materials and Catalysis Division, CSIR-Central Salt and Marine Chemicals Research Institute, Bhavnagar 364002, India*
[d]*Analytical and Environmental Science Division and Centralized Instrument Facility, CSIR – Central Salt and Marine Chemicals Research Institute, Bhavnagar 364 002, Gujarat, India*

† Electronic supplementary information (ESI) available. See DOI: https://doi.org/10.1039/d4eb00023d

These approaches involve membranes with proton selectivity and/or Donnan exclusion.[3]

Proton-selective membranes, generally cation-exchange membranes, are prepared by solvent evaporation and/or extrusion methods.[4] The development of membranes with Donnan exclusion involves anion-exchange membranes with tuned porosity, which selectively allows protons to pass through while excluding vanadium ions. However, at the commercial scale, perfluorinated membranes such as Nafion are dominant due to their excellent electrochemical and physicochemical properties, including exceptional oxidative stability in battery environments.[5] Nevertheless, the high vanadium ion crossover and high cost of these membranes have encouraged the search for alternatives.[6] Efforts have been made to modify perfluorinated membranes, either in bulk or at the surface, to reduce vanadium ion crossover; however, this has resulted in increased areal resistance of the membranes. Chien-Hong Lin *et al.* reported that a Nafion/amino-silica hybrid membrane exhibited lower vanadium ion permeabilities for VO^{2+} and VO_2^+ of 2.32×10^{-7} cm^2 min^{-1} and 0.85×10^{-7} cm^2 min^{-1} respectively. However, this modification also led to an increase in area resistance to 3.45 Ω cm^2, higher than that of the pristine Nafion-117® membrane.[7] This suggests that a trade-off between ion permeability and ohmic resistance must be maintained to achieve membranes with optimal properties.[8,9] This has led to efforts in developing hydrocarbon-based cation-exchange membranes, with particular interest in thermoplastic engineering materials such as poly(ether ether ketone) (PEEK), poly(ether sulfone) (PES), poly(phenylene oxide) (PPO), polystyrene (PS), poly(vinylidene fluoride) (PVDF), and polybenzimidazole (PBI). Although some encouraging results have been reported, the issue of vanadium ion permeability has not yet been adequately addressed.[10,11]

Hydrocarbon-based anion-exchange membranes capitalize on the Donnan exclusion principle to reduce vanadium ion cross-contamination. However, their poor ohmic resistance and chemical stability limit their utility.[12] Ohmic resistance has been lowered by using pore-filled membranes, while chemical stability has been enhanced with smart polymer matrices like polypropylene and polytetrafluoroethylene.[13,14] Additionally, proton exchange membranes containing basic functional groups have been extensively explored for VRFB applications. Notably, Ning Shi *et al.* developed a high-temperature proton exchange membrane for VRFB, representing cutting-edge advancements in energy conversion and storage.[15] Among these, the 1.5% TPB-PBAP membrane exhibited exceptional long-term cycling durability, maintaining stable EE after 300 cycles, the CE of the VRFB with the 1.5% TPB-PBAP membrane remained unchanged at 98.9%, while its EE showed only a slight decrease from 86.1% to 83.3%. Under the same conditions, the CE of Nafion 212 was 97.7%, with its EE decreasing from 84.5% to 81.6% after 300 cycles. Furthermore, a similar group fabricated a poly(isatin triphenyl) (PIT)-based membrane with a lactam structure and devoid of ether bonds which was synthesized *via* superacid catalysis. To improve ion transport, PIT is functionalized with both cationic and anionic side chains through ring-opening reactions using glycidyl trimethylammonium chloride (GTA) and 1,3-propane sultone (PS), resulting in an amphoteric membrane. This tailored structure effectively suppresses hydrated vanadium ion migration, enabling the VRFB assembled with PIT-GTA to achieve an extended prolonged self-discharge duration of 289 h, significantly outperforming Nafion 115 (86 h).[16] Although this method could address VRFB challenges, a robust membrane preparation method is still needed from a commercial perspective. This has driven the development of mixed matrix membranes, where hybridization of organic and inorganic material properties addresses these issues.[17]

Mixed matrix membranes (MMMs) have been extensively researched to modify the electrochemical and physicochemical properties of membranes.[18] By taking advantage of the flexibility of organic matrices and the functional and thermal stability of inorganic fillers, the properties of the membrane can be tailored to meet specific requirements.[19] In the preparation of ion-exchange membranes, commonly used inorganic fillers include silica (SiO_2), titanium dioxide (TiO_2), zirconium dioxide (ZrO_2), and titanosilicates, owing to their inherent proton-conducting ability and excellent thermal and chemical stability.[20,21] Other fillers, such as aluminum oxide, hexagonal boron nitride, niobium disulfide, and tungsten trioxide, are utilized for their high thermal stability.[22,23] Recently, porous materials like zeolites, metal–organic frameworks (MOFs), and covalent organic frameworks (COFs) have been chosen for their specific pore sizes and structural characteristics, which enhance membrane performance.[24,25] Zeolites, in particular, have gained significant attention as fillers due to their ion selectivity, which facilitate proton transport while preventing vanadium ion diffusion. Recently, Xia *et al.*[26] employed a flow-processing technique to prepare zeolite-based MMMs, aligning zeolite nanosheet fillers in a preferred orientation within a Nafion® polymer matrix. The resulting membrane exhibited high proton conductivity (80.1 mS cm^{-1}) and excellent vanadium ion selectivity (2.01×10^5 min cm^{-3}). A single-cell VRFB assembled with the zeolite-Nafion® composite membrane demonstrated high energy efficiency at an applied current density of 200 mA cm^{-2}. The same group later reported a zeolite-SPEEK composite membrane by synthesizing cross-linked zeolite nanosheets (ZN) functionalized with anionic and cationic groups, followed by incorporation into a sulfonated poly(ether ether ketone) (SPEEK) polymer matrix.[27] The resulting hybrid membranes exhibited significantly enhanced proton selectivity over vanadium ions, achieving a coulombic efficiency (CE) of 99.0% and an energy efficiency (EE) of 85.0% at an applied current density of 120 mA cm^{-2}, outperforming both pristine SPEEK and the state-of-the-art Nafion-212® under identical testing conditions. Cai *et al.*[28] prepared MMMs by incorporating ZSM-5 with varying Si–Al ratios into the SPEEK matrix, achieving significantly enhanced ion transport. The optimized membrane demonstrated superior performance, with a voltage efficiency (VE) of 85.7% and an EE of 85.1% at 120 mA cm^{-2}. Yang *et al.* developed a colloidal silicalite-Nafion composite membrane, leveraging sub-nanometer

zeolitic pores to enhance proton selectivity while blocking hydrated vanadium ions.[29] Recently, our group reported that proton-conducting zeolite significantly boosts proton conduction, thereby improving VRFB performance. The best-performing SPEEK-ZSM-5 (25) $2H^+$ achieved an average CE of 97.0% and an average EE of 78.0% over 300 charge/discharge cycles at a current density of 80 mA cm^{-2}.[30] The significant enhancement in proton conduction and vanadium ion exclusion has primarily relied on ion sieving through the pores of modified zeolites. Herein, we report a vanadium ion-encased modified zeolite to capitalize simple yet effective, '*like repels like*' theory in synergy with the ion sieving to achieve low vanadium diffusivity. The modified zeolite was infiltrated into the SPEEK polymer matrix to fabricate a high-performance membrane for VRFB. This facile and innovative modification of zeolite is an effective approach to substantially reduce the permeability of vanadium ions across the membrane thereby enhancing the overall efficacy of VRFB.

2. Experimental section

2.1 Materials

Poly(ether ether ketone) (PEEK), with an average molecular weight (M_w) of approximately 85 000 and a polydispersity index (PDI) of 2.64, was supplied by Solvay.[30] *N*,*N*-Dimethylacetamide (DMAc, 99%), isopropyl alcohol (IPA), and sulfuric acid (H_2SO_4, 98%) were obtained from Qualigens India. Vanadium oxychloride ($VOCl_3$, 99%), vanadium(IV) sulfate oxide hydrate ($VOSO_4{\cdot}5H_2O$, 96%), vanadium(V) oxide (98%), and vanadium(III) chloride (VCl_3, 97%) were purchased from Alfa Aesar. Magnesium sulfate ($MgSO_4$, 99%) and sodium chloride (NaCl, 99.9%) were procured from Research Lab India. The sodium forms of pentasil-type zeolite ZSM-5 (40) were provided by Zeochem LLC, Uetikon, Switzerland. Deionized (DI) water with a resistivity of 18.0 MΩ cm was used throughout the experiments.

2.2 Synthesis of vanadium encased zeolite samples

Vanadium-encased zeolite was prepared using an ion-exchange method followed by thermal sintering. Briefly, ZSM-5 (40)-Na^+ was treated with a 0.05 M acidic vanadium(V) oxide solution (prepared by dissolving 0.05 M vanadium(V) oxide in a 2.0 N sulfuric acid solution). The reaction mixture was stirred for 4 hours at 70 °C. To achieve maximum loading of vanadium ions, the process was repeated four times. Subsequently, the sample was washed with deionized water to remove excess ions from the zeolite's surface. The material was dried at 60 °C for 12 hours and then at 120 °C for 24 hours, followed by calcination at 550 °C for 10 hours with a ramp rate of 10 °C per minute up to 550 °C. The obtained zeolite was labeled as ZSM-5 (40)-VO_2^+.

2.3 Preparation of SPEEK-based mixed matrix membrane

Before preparing the mixed matrix membrane, PEEK was sulfonated in concentrated sulfuric acid as reported previously,[30] and designated as SPEEK. The mixed matrix membrane was prepared by physically blending ZSM-5 (40)-VO_2^+ with SPEEK. Briefly, ZSM-5 (40)-VO_2^+ (100.0 mg) was dispersed in 5.0 mL of DMAc using ultrasonication. Separately, a 10.0% SPEEK solution in DMAc was prepared. The zeolite dispersion was slowly added to the SPEEK solution and stirred for 8 hours. The resulting mixture was cast onto a glass plate and dried overnight at 60 °C. The glass substrate was then submerged in deionized water to peel off the membrane from the glass surface. The resulting membrane was labeled as SPEEK-ZSM (40) VO_2^+. For comparative studies, SPEEK-ZSM (40) Na^+ and neat SPEEK membranes were prepared using the same procedure, with and without the addition of ZSM-5 (40)-Na^+, respectively. The membranes were stored in a saline solution for further analysis and battery application.

2.4 Characterization

2.4.1 Degree of sulphonation. The degree of sulfonation (DS) of the SPEEK polymer was determined *via* acid–base titration using a standardized 0.1 N NaOH solution in *N*,*N*-dimethylformamide (DMF). A 0.5 g sample of SPEEK polymer was dissolved in 10 mL of DMF, and the resulting solution was titrated with NaOH, using phenolphthalein as an indicator. The volume of NaOH required for neutralization was then used to calculate the DS of the SPEEK polymer, as expressed in the following eqn (1).[31]

$$\mathrm{DS} = \frac{0.291 \times M_{\mathrm{NaOH}} \times V_{\mathrm{NaOH}}}{W - 0.081 \times M_{\mathrm{NaOH}} \times V_{\mathrm{NaOH}}} \times 100 \quad (1)$$

where $V_{(\mathrm{NaOH})}$ is the volume of the NaOH solution used for neutralization (mL), and $M_{(\mathrm{NaOH})}$, is the molarity (mol L^{-1}) of the standard NaOH solution. W is the mass of SPEEK polymer, the molecular weight of a single repeating unit of PEEK polymer is 291 g mol^{-1} and the molecular weight of the sulphonic acid (SO_3H) functional group is 81 g mol^{-1}.

The DS was determined to be 38.64% using this method.

2.4.2 Water uptake (WU). The membrane's water uptake (WU) was determined using the gravimetric method. A membrane piece (2 × 2 cm) was immersed in DI water for 24 h, and its wet weight (M_{wet}) was determined after wiping off excess surface water. After drying the membrane at 60 °C for 24 h, then dry weight (M_{dry}) was measured. Water uptake (%) was calculated using the following eqn (2):[32]

$$\mathrm{WU} = \frac{M_{\mathrm{wet}} - M_{\mathrm{dry}}}{M_{\mathrm{dry}}} \quad (2)$$

2.4.3 Ion exchange capacity (IEC). The Ion Exchange Capacity (IEC) is a crucial parameter that quantifies the number of exchangeable functional groups in a membrane. Its estimation involves proton exchange with sodium ions, followed by acid–base titration. Initially, three identical membrane samples (2 × 2 cm) are treated with 1.0 M HCl for 24 hours to convert all ion-exchange sites to the proton (H^+) form, ensuring consistent starting conditions for IEC measurement. Subsequently, the membrane pieces are immersed in a

1.0 M NaCl solution for 24 hours, allowing the H^+ ions to be exchanged with Na^+ ions from the solution. The concentration of H^+ ions in the solution is then determined by titration against a standardized NaOH solution, using phenolphthalein as an indicator. The volume of NaOH consumed during titration is used to calculate the IEC of the membrane, as expressed in eqn (3).[33]

$$\mathrm{IEC} = \frac{C \times V}{M_{\mathrm{dry}}} \quad (3)$$

where C represents the concentration of solution present in the burette, V is the volume consumed during titration, and M_{dry} is the dry weight of the membrane.

2.4.4 Ionic conductivity. The membrane's conductivity was evaluated through impedance spectroscopy measurements carried out using a custom-built conductivity cell with an active area of 1.0 cm^2. These measurements were performed with a CHI 700E potentiostat/galvanostat. The membrane resistance was extracted from the simulated circuit model, and this resistance was subsequently used to calculate the membrane's conductivity, as per eqn (4).[34]

$$\sigma = \frac{L}{R \times A} \quad (4)$$

Here, σ represents the conductivity in Siemens per centimeter (S cm^{-1}), L denotes the distance between the electrodes, which corresponds to the membrane thickness (cm), A is the active area of the membrane (cm^2), and R (Ω) is the measured resistance of the membrane.

2.4.5 Spectroscopy characterization. The surface morphology of the materials and membranes was thoroughly analyzed using a JEOL JEM 7100F Field Emission Scanning Electron Microscope (FESEM). The integrity of the crystallographic structure of the zeolite was determined using an Empyrean-Analytical Powder X-ray Diffraction (XRD) instrument. The thermal behavior of the membranes was assessed through Thermogravimetric Analysis (TGA) utilizing a NETZSCH TG 209F1 Libra TGA instrument. The experiments were conducted under a controlled inert atmosphere, with TGA analysis involving heating the membrane from ambient temperature to 800 °C in nitrogen. The glass transition temperature of the membranes was determined using Differential Scanning Calorimetry (DSC) with a NETZSCH instrument, conducted over a temperature range of 25 °C to 250 °C. Mechanical properties, including tensile strength and elasticity of the membranes, were evaluated using a Zwick Roell BT-FR 2.5TH 40 Universal Testing Machine (UTM). Surface area and pore characteristics were investigated using a Micromeritics Smart VacPrep system, followed by detailed analysis with a Micromeritics 3 Flex version 4.03 instrument. The membrane underwent a thorough 4 hour degassing process at 250 °C to ensure accuracy in determining surface area, pore size, and pore volume; an important parameters for its functional performance. The elemental composition of zeolite samples was analyzed *via* X-ray Photoelectron Spectroscopy (XPS) using an ESCALAB instrument. Vanadium metal ion concentrations were quantified through Inductively Coupled Plasma Mass Spectrometry (ICP-MS) using Thermo Scientific's iCAP RQ device, providing precise measurements of elemental states and concentrations within the membrane.

2.5 Vanadium ion permeability study

The diffusion of vanadium ions across the membrane was investigated using a conventional two-compartment cell setup, as reported in the literature.[35] To maintain charge balance in the solution, as previously reported for VO^{2+}, the system consisted of (VO^{2+}: 1 M $VOSO_4$ + 1.6 M H_2SO_4||1 M $MgSO_4$ + 1.6 M H_2SO_4). Similar procedures have been applied in studies involving other vanadium ions, such as VO_2^+ and V^{3+}.[3] The solutions in both compartments were stirred using magnetic beads to reduce the concentration polarization effect at the membrane surface. Vanadium ion permeability was quantified by monitoring concentration changes over time using inductively coupled plasma (ICP) analysis of periodically collected samples.

2.6 Single-cell VRFB performance

The battery performance of the prepared composite membranes was rigorously examined using a single-cell redox flow battery with a 25 cm^2 active area, utilizing a battery testing setup from Neware. In this study, equal concentrations and volumes of positive (1.0 M VO^{2+} in 30 mL of 2.0 M H_2SO_4) and negative (1.0 M V^{3+} in 30 mL of 2.0 M H_2SO_4) electrolytes were continuously circulated at a flow rate of 50 mL min^{-1}. Key performance parameters, including coulombic efficiency (CE), voltage efficiency (VE), energy efficiency (EE), and capacity retention, were calculated based on established methodologies.[3,30] The self-discharge behavior of the membrane was also assessed at 100% state of charge (SOC) using a 12 cm^2 active area battery cell. The battery was initially charged at 1.6 V and 20 mA cm^{-2}, then allowed to self-discharge until the voltage decreased to 1.0 V. Polarization curves were recorded using a custom-built flow battery cell with a 12 cm^2 active membrane area. The battery cell was fully charged at a current density of 50 mA cm^{-2} to achieve a 100% SOC. Subsequently, controlled discharge experiments were conducted across a range of current densities from 25 to 475 mA cm^{-2}, with the cell potential monitored at each discharge step.

3. Results and discussion

Before the preparation of the mixed matrix membrane, zeolite (ZSM-5 (40)-Na^+) and its modification with vanadium ions (ZSM-5 (40)-VO_2^+) were thoroughly characterized for their structural integrity. Fig. 1 presents the powder XRD diffractograms of ZSM-5 (40)-Na^+ and ZSM-5 (40)-VO_2^+, along with the corresponding JCPDS file number (JCPDS: 44-0003).[36]

The identical peak positions for the majority of peaks indicate that the structural integrity of the material remained intact even after repeated ion exchange and thermal treatment.[37]

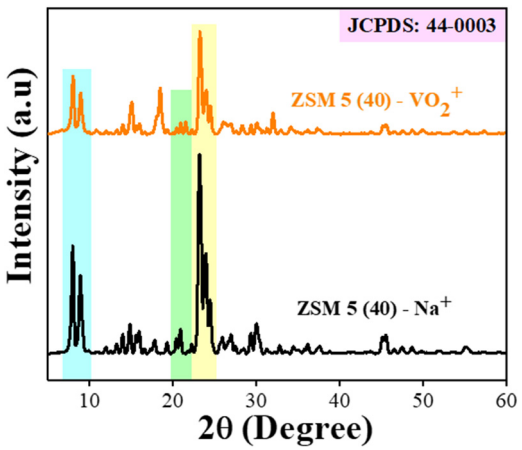

Fig. 1 Depicts the XRD pattern for ZSM-5- (40) with Na^+ and ZSM-5-(40) with VO_2^+.

The presence of vanadium (VO_2^+) ions in the extraframework of ZSM-5 zeolite was confirmed by X-ray Photoelectron Spectroscopy (XPS). Fig. 2(a–d) shows the XPS spectra of ZSM-5 (40)-Na^+ and ZSM-5 (40)-VO_2^+. The ZSM-5 (40)-Na^+ exhibited peaks at 103 eV (Si 2p orbital) for silicon (Fig. 2a), at 74 eV (Al 2p orbital) for aluminium (Fig. 2b), and 530 eV and 532.5 eV in the O_{1s} spectrum (Fig. 2c) for oxygen, confirming their presence.[38] The two types of oxygen come from Si–O and Al–O bonds. The oxygen bonded to silica was assigned to 532.5eV, while the oxygen bonded to aluminium was assigned to 530.8 eV. Additionally, a peak at 1072 eV corresponds to the Na_{1s} orbital, indicating the presence of sodium ions in the extraframwork sites of the zeolite (Fig. 2d).[39] Fig. 2(e–h) illustrates the XPS spectra of the VO_2^+-exchanged ZSM-5 zeolite, showing the presence of vanadium(v) alongside silicon (Si), aluminum (Al), and oxygen (O). The XPS analysis reveals a significant peak at 516.5 eV, corresponding to the $V2p_{3/2}$ orbital, indicating the presence of a V^{5+} oxidation state (Fig. 2h).[40] The Si_{2p} peak at 103 eV and the Al_{2p} peak at 74 eV[41] remain consistent with those of ZSM-5 (40)-Na^+ (Fig. 2e and f), suggesting that the silicon and aluminium environments are largely unaffected by the ion exchange process. Interestingly, a new peak was observed in the O_{1s} spectrum (Fig. 2g) at 529 eV, corresponding to the V–O bond.[42]

This indicates that V^{5+} is present in the VO_2^+ form.[43]The uniform distribution of VO_2^+ throughout the zeolite was visualized by SEM analysis combined with elemental mapping. Agglomerated particles with a typical morphology of ZSM 5[44] and an average particle size of 1μm were observed in the SEM images (Fig. 3a and e). No structural damage or degradation of the particles was observed after ion exchange followed by thermal sintering in ZSM-5 (40)-VO_2^+, indicating the robustness of the methodology and the structural integrity of the zeolite (Fig. 3b and f). Elemental mapping confirms the substitution of Na^+ ions in the extraframwork with VO_2^+ ions. (Fig. 3h), with a weight percentage of 2.30%. This value is higher than the expected amount for vanadium species replacing sodium ions, possibly due to VO_2^+ species within the pore volume or free space in the zeolite. ESI Fig. 1a, b, and c† validate the presence of Si, Al, and O in ZSM-5 (40)-Na^+, with its overall elemental composition determined as 1.29 wt% sodium (Na), 38.55 wt% silicon (Si), 1.79 wt% aluminum (Al), and 58.38 wt% oxygen (O) (Fig. 3c and d). Similarly, elemental mapping in ESI Fig. 1d, e, and f† confirms the distribution of Si, Al, and O in ZSM-5 (40)-VO_2^+, with corresponding weight percentages of 37.55% for Si, 1.02% for Al, and 59.13% for O (Fig. 3g). This combined data offers a comprehensive sight of the elemental distribution and confirms the uniform presence of these elements within the ZSM-5 framework. Additionally, the integrity of the zeolite after chemical modification was evaluated based on changes in surface area, pore size, and

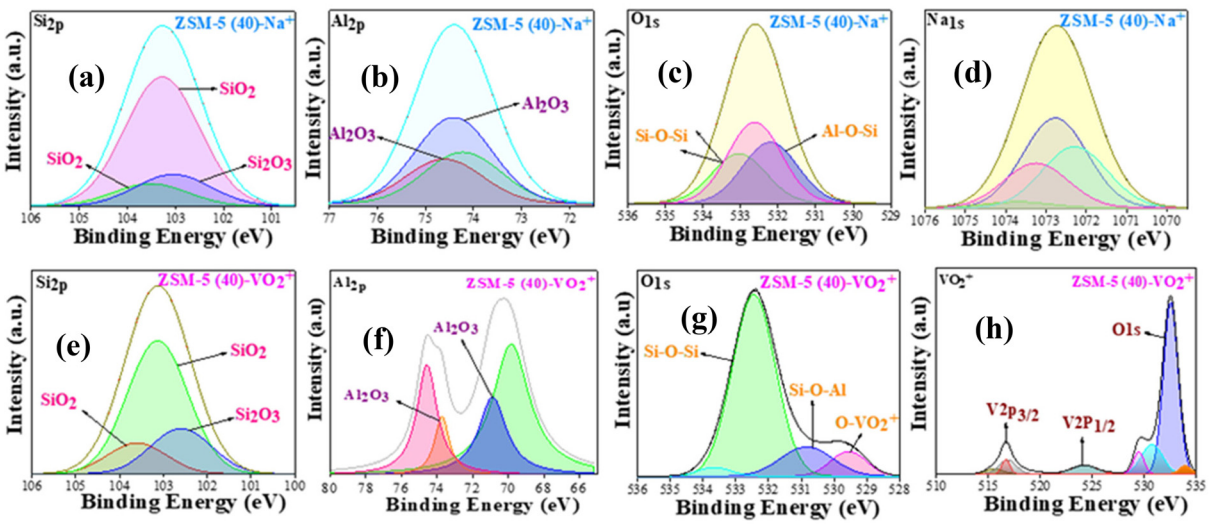

Fig. 2 XPS analysis of ZSM-40 zeolite samples (a), (b), (c), and (d) indicate the elemental composition of ZSM-40-Na^+ for Si, Al, O, and Na, respectively. (e), (f), (g), and (h) represent the elemental composition of ZSM-40-VO_2^+ for Si, Al, O, and VO_2^+, respectively.

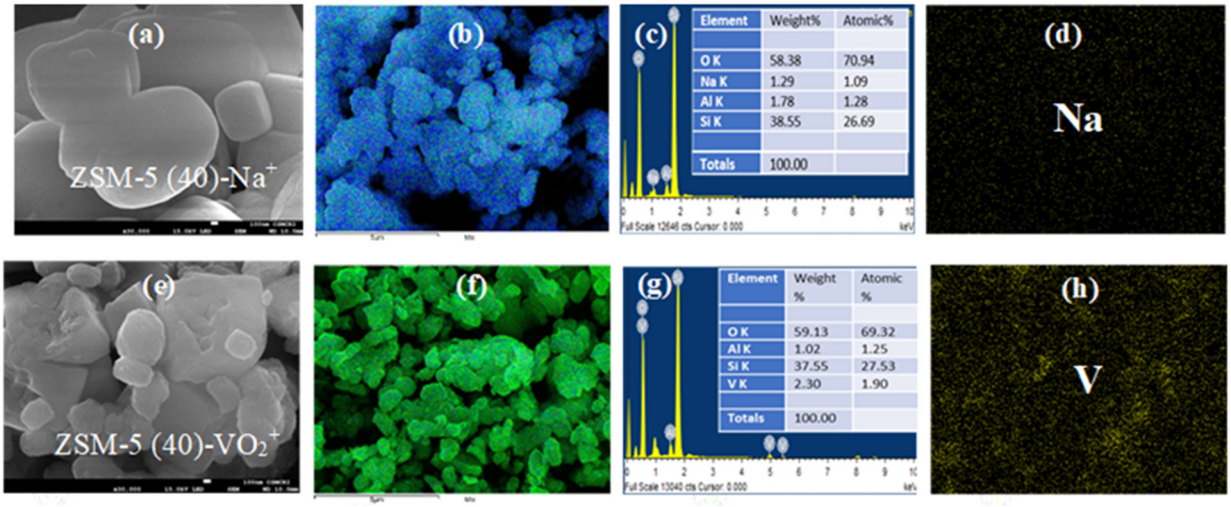

Fig. 3 SEM images and elemental mapping of zeolite samples: (a) SEM Image of ZSM-5 40-Na^+; (b) elemental mapping of ZSM-5 40-Na^+; (c) table elemental mapping of ZSM-5 40-Na^+; (d) elemental mapping of Na in ZSM-5 40-Na^+; (e) SEM Image of ZSM-5 40-VO_2^+; (f) elemental mapping of ZSM-5 40-VO_2^+; (g) table elemental mapping of ZSM-5 40-VO_2^+; (h) elemental mapping of VO_2^+ in ZSM 5 40-VO_2^+.

pore volume. Table 1 shows the measured values for surface area, pore volume, and pore size. The ZSM-5 (40)-Na^+ had a pore size of 4.2 nm and a surface area of 352.6 $m^2\ g^{-1}$, whereas ZSM-5 (40)-VO_2^+showed a pore size of 4.8 nm and a surface area of 387.0 $m^2\ g^{-1}$. The increase in pore size and surface area for the vanadium-modified zeolite can be attributed to the expansion of the zeolite framework by VO_2^+ ions. The introduction of VO_2^+ ions promotes the reorganization of structure to maintain stability.[45] This reorganization increases pore size due to the creation of vacancies or defects, leading to a more open framework.[46] However, the expansion is relatively small, which helps maintain the structural integrity of the zeolite.

Following the confirmation of the formation of ZSM-5 (40)-VO_2^+, a mixed matrix membrane was prepared by simply physically blending ZSM-5 (40)-$VO_2^+$with SPEEK. This membrane was designated as SPEEK-ZSM 40 VO_2^+. For comparison purposes, neat SPEEK and a mixed matrix membrane of SPEEK and ZSM-5 (40) Na^+, designated as SPEEK-ZSM 40 Na^+, were also prepared and evaluated under identical experimental conditions.

Fig. 4 presents the characterization of the prepared membranes: (a), (b), and (c) show the optical images of SPEEK-48, SPEEK-ZSM 40 Na^+, and SPEEK-ZSM 40 VO_2^+, respectively. All three membranes exhibit a homogeneous, compact, and dense structure. The pure SPEEK-48 membrane appears colourless, while the composite membranes show a colour change to white for SPEEK-ZSM 40 Na^+ and yellow for SPEEK-ZSM 40 VO_2^+, indicating successful modification. Furthermore, the SEM analysis (a′, b′, and c′) highlights the strong compatibility between SPEEK and the zeolite, as evidenced by the uniform dispersion of zeolite particles throughout the polymer matrix without significant phase separation.[47] This compatibility arises from the chemical interactions between the sulfonic acid groups of SPEEK and the surface functional groups of the zeolite, promoting effective adhesion at the polymer-filler interface. The absence of voids or agglomeration in the SEM images further supports the homogeneous distribution of the filler, indicating good interfacial bonding.[48] The EDX analysis, shown in (a″), (b″), and (c″), confirms the incorporation of zeolite into the SPEEK polymer matrix by detecting characteristic elemental signals. This strong compatibility not only enhances the membrane's structural integrity but also ensures efficient ion transport pathways, crucial for VRFB application.

Table 1 Specific Surface Area, Pore Volume, and Average Pore Size of ZSM-5 Zeolite Samples

Zeolite code	Specific area ($m^2\ g^{-1}$)	Pore volume ($cm^3\ g^{-1}$)	Pore size (nm)
ZSM-5 (40)-Na^+	352.6	0.148	4.2
ZSM-5 (40)-VO_2^+	387.0	0.145	4.8

The evaluation of the membranes began with measurements of ion exchange capacity (IEC) and water content (WU). SPEEK-48 exhibited an IEC of 1.25 meq g^{-1}, which was higher than SPEEK-ZSM 40 Na^+ (1.15 meq g^{-1}) and SPEEK-ZSM 40 VO_2^+ (1.11 meq g^{-1}). The lower IEC value for SPEEK-ZSM 40 VO_2^+ was attributed to non-exchangeable VO_2^+ ions occupying the exchangeable proton sites, reducing the accessibility of ion exchange sites.[49] This is further confirmed with ESI Fig. 2† by XPS analysis of the SPEEK-ZSM 40 VO_2^+ membrane, which suggests that vanadium ions are anchored at the sulfonic acid sites within the SPEEK backbone, as evidenced by the observed shifts in binding energy, indicating their coordination and interaction within the polymer matrix. The ESI Fig. 2 a, b, and c† indicating V_{2p}, O_{1s}, and S_{2p} peaks respectively, suggest changes in the electronic environment due to vanadium coordination with sulfonic ($-SO_3H$) groups in SPEEK. The O_{1s} peaks at 532.29, 532.25, 531.29, and 533.29 eV suggest contributions from sulfonic acid, water, and vanadium–oxygen interactions, with shifts compared to pure SPEEK implying

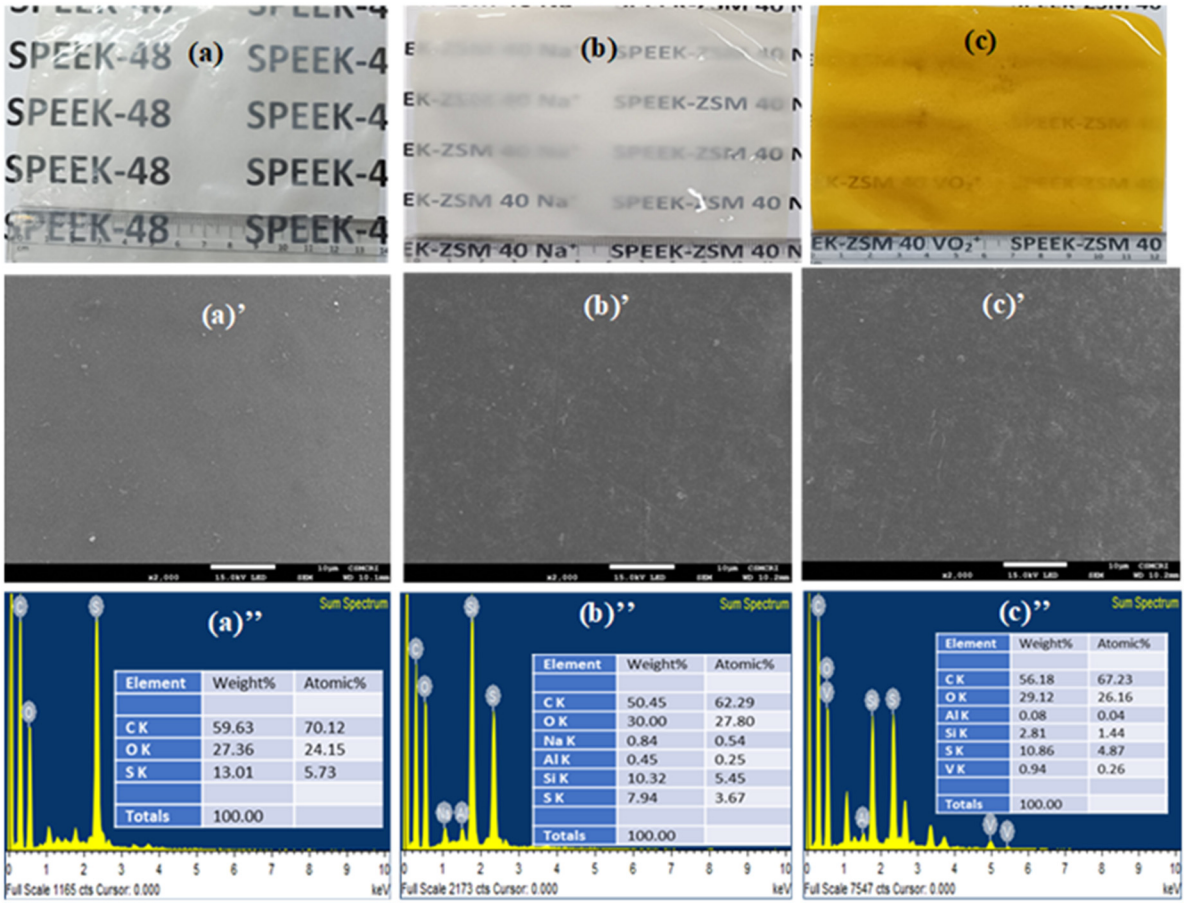

Fig. 4 (a), (b), and (c) present the optical images of the prepared membranes: SPEEK-48, SPEEK-ZSM 40 Na^+, and SPEEK-ZSM 40 VO_2^+ respectively. The corresponding surface morphologies are shown in (a′), (b′), and (c′), while (a″, (b″), and (c″) display the EDX analysis of the SPEEK-48, SPEEK-ZSM 40 Na^+, and SPEEK-ZSM 40 VO_2^+ membranes, respectively.

vanadium incorporation.[50] The V_{2p} peaks, if slightly shifted from standard vanadium oxides, further support vanadium-sulfonic interactions through electron donation. The shift in binding energy from ~163 to 168 eV in the S_{2p} peak may confirm the presence of a new chemical environment, indicating vanadium binding through ion exchange or coordination while maintaining the sulfate structure.[51] These binding energy shifts collectively indicate S–O–V interactions, reinforcing vanadium's integration into the SPEEK matrix, which could enhance ion transport properties in VRFB. A similar trend was observed for water uptake, with SPEEK-48 exhibiting 38.0% WU, while SPEEK-ZSM 40 Na^+ and SPEEK-ZSM VO_2^+ exhibited WU of 32.0% and 30.0%, respectively. It followed the measurement of ionic conductivity of the membranes in de-ionized (DI) water and 0.1 M H_2SO_4. The impedance spectra are presented in (ESI Fig. 3†). From these spectra, the calculated ionic conductivity values were 4.69, 6.25, and 8.33 mS cm^{-1} for SPEEK-48, SPEEK-ZSM 40 Na^+, and SPEEK-ZSM 40 VO_2^+ in DI water, respectively. In 0.1 M H_2SO_4, the conductivity values increased to 10.30, 16.00, and 18.18 mS cm^{-1} for SPEEK-48, SPEEK-ZSM 40 Na^+, and SPEEK-ZSM 40 VO_2^+, respectively. In the case of ion-exchange membranes, the water content and IEC usually exhibit a linear relationship with ionic conductivity *i.e.*, as IEC and water content increase, ionic conductivity typically increases. However, this trend is contradicted in the present study. With the addition of zeolite, the decrease in IEC and water content was due to the reduction in exchangeable protons, as VO_2^+ occupied the exchangeable proton sites. The increase in conductivity is associated with proton conduction through VO_2^+ ions residing in defined ion-conducting channels. It is well established in the literature[52] that the exfoliated layers of V_2O_5 form ion channels with excellent nanofluidic transport properties, exhibiting remarkable proton conductivity (~0.01 S cm^{-1}). The activation energy for proton conduction (0.066 eV) through V_2O_5 suggests a high mobility of H^+ ions (5.2×10^{-3} cm^2 V^{-1} s^{-1}) within the ion channels, facilitated by the coordinated hopping of protons between water molecules arranged in a two-dimensional structure. This may contribute to the observed increase in conductivity.

Fig. 5a shows the thermal stability of the mixed matrix membranes, which undergo degradation in three distinct steps. The first degradation, occurring at around 150 °C, is associated with the loss of bound and trapped water molecules in the membrane. The SPEEK- 48 membrane exhibited a weight loss of ~10%, while the SPEEK-ZSM 40 Na^+ and

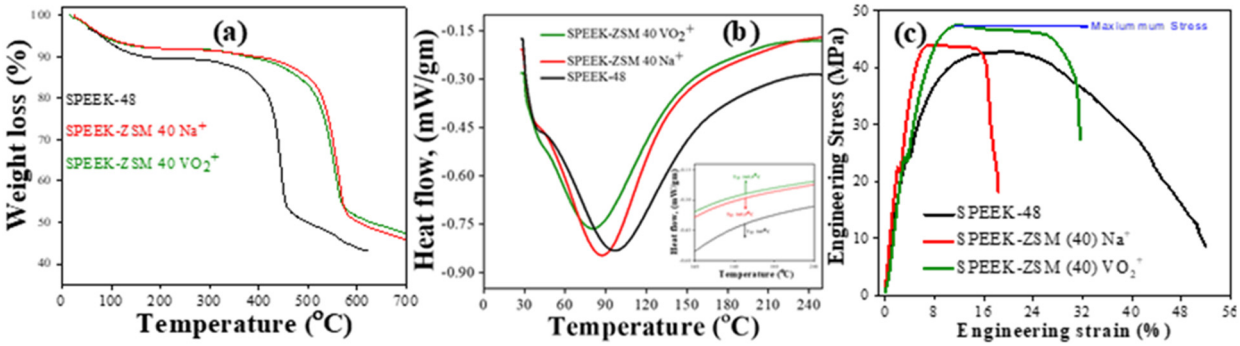

Fig. 5 Indicating (a) thermal stability of the membrane *via* thermogravimetric analysis; (b) DSC (c) mechanical strength of the membrane *via* UTM analysis.

SPEEK-ZSM 40 VO_2^+ membranes showed 8.2% and 8.4%, respectively. The lower weight loss in the mixed matrix membranes is attributed to the retention of intercrystallite water by the zeolite molecules.[53] The second weight loss was observed beyond 300 °C and is attributed to the desulfonation of the polymer matrix. The SPEEK-48 membrane exhibited a weight loss of at ~300 °C, whereas the mixed matrix membranes exhibited weight loss beyond ~380 °C. The increased temperature of the second weight loss is due to interactions between the silica-alumina framework of the zeolite and the sulfonic acid groups of the polymer matrix. The third degradation step involves the breakdown of the polymer backbone, occurring beyond 400 °C. SPEEK-48 begins to degrade around 400 °C, while the mixed matrix membranes show delayed degradation, with an onset temperature of approximately 590 °C due to the presence of zeolite filler. Fig. 5b shows the DSC analysis of the membranes. The observed glass transition temperatures (T_g) are 165 °C, 165.5 °C, and 165.9 °C for the SPEEK-48, SPEEK-ZSM 40 Na^+, and SPEEK-ZSM 40 VO_2^+ membranes, respectively. This indicates that the zeolite filler has a negligible effect on the T_g of the membrane, but it may substantially enhance thermal stability.

Fig. 5c shows the stress–strain properties of the membranes. The SPEEK-48 membrane exhibited a tensile strength of 42.39 MPa and a strain of 51.66%, while the SPEEK-ZSM 40 Na^+ membrane showed a tensile strength of 43.56 MPa and a strain of 20.56%. The SPEEK-ZSM 40 VO_2^+ membrane demonstrated a tensile strength of 47.26 MPa and a strain of 28.83%. The observed increase in mechanical strength of the SPEEK-zeolite composite membranes can be attributed to the formation of hydrogen bonds between the sulfonic acid groups ($-SO_3H$) in the SPEEK polymer and the hydroxyl groups on the surface of the zeolite particles.[54] These hydrogen bonds result in strong interfacial interactions, enhancing the adhesion between the polymer matrix and the filler, thereby improving the overall mechanical properties of the membrane.

The oxidative stability of the membranes was evaluated by immersing them in a 1.5 M VO_2^+ solution in 2.0 M H_2SO_4 and monitoring changes in weight and dimensions every 24 hours for 20 consecutive days. Detailed data on the weight and dimensional changes of the membranes, along with the measured IEC, WU, and mechanical strength after the oxidative stability test, are presented. Fig. 6(a) observed changes in weight and dimensions were 17.90% and 15.64%, 12.65%

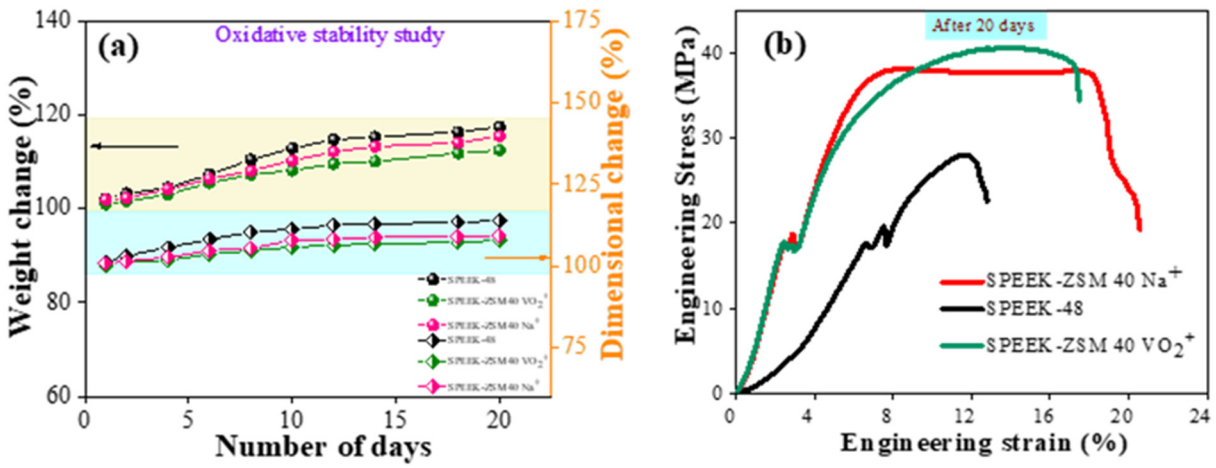

Fig. 6 (a) Weight and dimension change study of the SPEEK-48, SPEEK-ZSM 40 Na^+ and SPEEK-ZSM 40 VO_2^+ immersed in VO_2^+ ion solution in H_2SO_4. (b) UTM analysis of the membrane after oxidative stability testing.

and 13.8%, 9.3%, 7.8% for the SPEEK-48, SPEEK-ZSM 40 Na^+, and SPEEK-ZSM 40 VO_2^+ membranes, respectively. The observed increase in both weight and dimensions can be attributed to the adsorption or exchange of VO_2^+ ions with the sulfonic acid groups of the membrane. As VO_2^+has a significantly higher molecular weight than protons (H^+), this ion exchange leads to a noticeable increase in membrane mass, particularly during the initial stages of immersion.[4,33] These results suggest that the zeolite filler does not adversely affect membrane stability and slightly decreases weight change. This is due to the repulsive interactions between the VO_2^+ ions in the membrane matrix and solution.[55] The encapsulated vanadium in the zeolite repels the external vanadium ions, protecting the polymer backbone from degradation and thereby enhancing oxidative and thermal stability. Fig. 6(b) shows the stress–strain curves of the membranes following the oxidative stability study. The SPEEK-48 membrane exhibited a significant reduction in tensile strength from 42.39 MPa to 27.45 MPa, along with a decrease in strain from 51.66% to 22.99%, representing approximately 35.24% loss in mechanical strength. In contrast, the SPEEK-ZSM 40 Na^+ and SPEEK-ZSM 40 VO_2^+ membranes showed tensile strengths and strains of 37.97 MPa and 20.98%, and 40.53 MPa and 36.15%, respectively, indicating only about ~13% and 14% decrease in mechanical strength.

These results suggest that the incorporation of ZSM-5 40-Na^+ and ZSM-5 40-VO_2^+ into the membrane matrix significantly enhances its oxidative stability. (Fig. 7) illustrates the infiltration of ZSM-5 (40)-VO_2^+ into the SPEEK polymer matrix, highlighting the Donnan exclusion of vanadium ions while allowing selective proton permeation. This effect is more pronounced for the ZSM-5 40-VO_2^+, likely due to repulsive interactions, specifically Donnan exclusion, between the VO_2^+ ions present in the solution and in the membrane matrix. Table 2 presents the IEC and WU values of the membranes after the oxidative stability test. A SPEEK-ZSM-5 40-VO_2^+ membrane shows decrease of approximately 18% in IEC and 6% in WU was observed. The observed decreases in IEC and WU are primarily attributed to fouling of the polymer matrix by VO_2^+ molecules, which occupy the exchangeable proton sites of the sulfonic acid groups, affecting both IEC and WU. Unlike protons, VO_2^+ ions do not participate in ion exchange processes, resulting in a lower IEC. Furthermore, the presence of vanadium species in the polymer matrix reduces its ability to absorb water, thereby decreasing the WU.[56]

Table 2 Represents the IEC and WU of the SPEEK membranes pre and post-oxidative stability

Membranes	Pre-oxidative stability		Post oxidative stability	
	IEC (meq g^{-1})	WU (%)	IEC (meq g^{-1})	WU (%)
SPEEK-48	1.25	38	0.91	29
SPEEK-ZSM 40 Na^+	1.15	32	0.87	27
SPEEK-ZSM 40 VO_2^+	1.11	30	0.90	28

3.1 Vanadium ion permeability

Understanding the detailed behavior of vanadium ion diffusion through membranes is crucial for optimizing the performance of a VRFB (Vanadium Redox Flow Battery). The vanadium ion diffusion coefficients were evaluated in a two-compartment cell, as reported in our earlier study,[30] and the corresponding data are presented in Table 3. The SPEEK-ZSM 40 VO_2^+ membrane exhibited diffusion coefficients of 3.93×10^{-7}, 5.12×10^{-7}, and 2.98×10^{-7} cm^2 min^{-1} for V^{3+}, VO^{2+}, and VO_2^+ions, respectively. These values are lower than those for the SPEEK-48 and SPEEK-ZSM 40 Na^+ membranes, which

Table 3 Vanadium ions diffusion coefficient across the membranes

Membranes	V^{3+} (cm^2 min^{-1})	VO^{2+} (cm^2 min^{-1})	VO_2^+ (cm^2 min^{-1})
SPEEK-48	3.55×10^{-6}	4.88×10^{-6}	3.13×10^{-6}
SPEEK-ZSM (40) Na^+	4.12×10^{-7}	5.39×10^{-7}	3.85×10^{-7}
SPEEK-ZSM (40) VO_2^+	3.93×10^{-7}	5.12×10^{-7}	2.98×10^{-7}

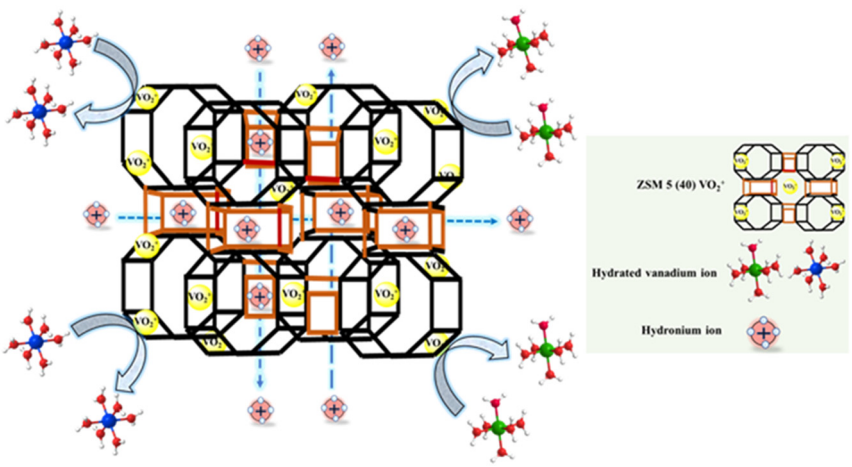

Fig. 7 Cartoon presentation of the ZSM-5 40-VO_2^+ zeolite demonstrating Donna exclusion of vanadium ions and selective permeation of protons.

showed diffusion coefficients of 3.55×10^{-6}, 4.88×10^{-6}, and 3.13×10^{-6} cm^2 min^{-1}, as well as 4.12×10^{-7}, 5.39×10^{-7}, and 3.85×10^{-7} cm^2 min^{-1} for V^{3+}, VO^{2+}, and VO_2^+ ions, respectively. These values are lower than those of Nafion-117®, which exhibited a vanadium ion diffusion coefficient of 5.73×10^{-6} cm^2 min^{-1}.[57] Yun Li *et al.* reported a coefficient of 4×10^{-6} cm^2 min^{-1} for polyether sulfone membranes. The addition of PVP in casting solutions increased membrane porosity, reducing area resistance and improving vanadium ion permeability. Wenping Wei *et al.* fabricated PVDF/M-23-125 membranes with a lower diffusion coefficient (7.9×10^{-7} cm^2 min^{-1}), while Lihui Wang *et al.* reported a similar value for polybenzimidazole-based membranes (5.74×10^{-7} cm^2 min^{-1}). This suggests that the synthesized mixed matrix membrane demonstrates excellent proton selectivity over hydrated vanadium ions.[11] The reduced diffusion coefficients for the SPEEK-ZSM 40 VO_2^+ membrane can be attributed to the synergistic effects of proton selectivity and Donnan exclusion. The zeolite pores selectively restrict the movement of ions but allow protons to pass through, while VO_2^+ ions experience Donnan exclusion of vanadium ions. The diffusion behaviour of VO_2^+ ions have been widely explored in the literature, largely due to the formation of neutral $VOSO_4$ complexes, which face minimal repulsion from the charged membrane matrix, enabling easier diffusion.[58] However, in the case of the SPEEK-ZSM 40 VO_2^+ membrane, significant repulsion is observed, resulting in lower diffusion coefficients.

3.2 Single-cell VRFB performance

Before evaluating battery performance, the polarization curve of the membrane was recorded to illustrate the relationship between cell voltage and current density. Fig. 8(a) presents the polarization curves for Nafion-117®, SPEEK-48, SPEEK-ZSM 40 Na^+, and SPEEK-ZSM 40 VO_2^+ membranes, demonstrating the combined losses of the cell: namely, losses associated with activation, concentration polarization, and mass transfer,[59] which strongly influences the membrane's polarization curve. The observed peak power density for Nafion-117®, SPEEK-48, SPEEK-ZSM 40 Na^+, and SPEEK-ZSM 40 VO_2^+ membranes was 285.75, 293.25, 305.91, and 330.45 mW cm^{-2}, respectively. The elevated peak power density of the SPEEK-ZSM-40 VO_2^+ membrane is attributed to improved proton conductivity in the acidic electrolyte of the VRFB. This high proton conductivity is induced by the membrane's structure, which facilitates efficient proton transport through its zeolitic channels. Fig. 8(b) presents a comparative analysis of self-discharge for SPEEK-48, SPEEK-ZSM 40 Na^+, SPEEK-ZSM 40 VO_2^+, and Nafion-117® membranes at 100% state of charge. The time taken for complete discharge of the cell was 401, 408, 476, and 533 minutes for Nafion-117®, SPEEK-48, SPEEK-ZSM-40 Na^+, and SPEEK-ZSM-40 VO_2^+ membranes, respectively. These values align with the diffusion of vanadium ions across the membranes. The longer discharge time of 533 minutes for the SPEEK-ZSM-40 VO_2^+ membrane is associated with its lower diffusion coefficient. The vanadium-encased zeolite within the SPEEK matrix plays a pivotal role in reorganizing the ionic pathways. It enhances proton selectivity and creates a more tortuous path for hydrated vanadium species through the SPEEK matrix, effectively reducing vanadium ion crossover. The extra-framwork vanadium ions within the zeolite amplify Donnan exclusion effects, limiting excessive diffusion of vanadium ions. Additionally, by adsorbing hydrated vanadium ions onto the sulfonic acid sites of the SPEEK matrix, the vanadium-encased zeolites create competition for charge-balancing sites, effectively reducing self-discharge in the battery.[30]

The performance of the membranes in the VRFB was evaluated using a single cell with an effective area of 25 cm^2. Fig. 9 presents the rate performance of the membranes at various current densities. The data suggest that at higher current densities, the shortened charge–discharge time aids in restricting the movement of excess vanadium ions across the membrane, thereby minimizing undesired crossover between half-cells and enhancing CE. Since ion diffusion is a major contributor to capacity loss, the reduced diffusion of vanadium ions at higher current densities minimizes self-discharge, decreases energy losses, and ultimately enhances CE.[55] A comparison of CE in Fig. 8a shows that the Nafion-117® membrane exhibits lower CE compared to the SPEEK-48, SPEEK-ZSM 40 Na^+, and

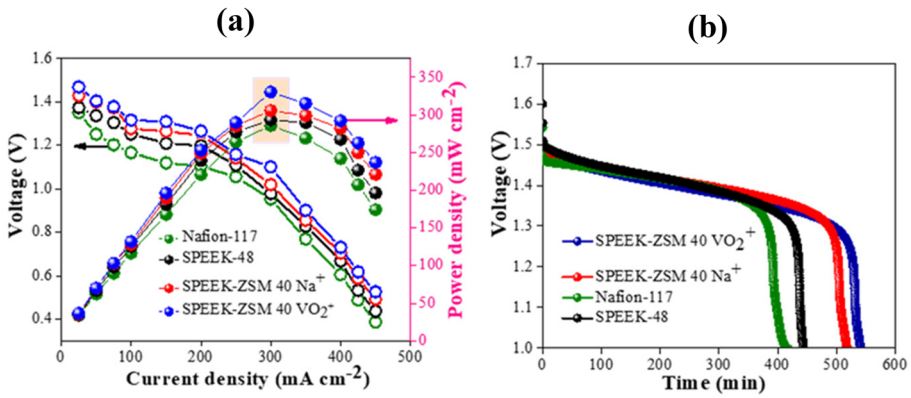

Fig. 8 Single cell performance VRFB (a) shows the polarization curve and (b) self-discharge study of the SPEEK-Zeolite composite membrane along with Nafion-117® membrane.

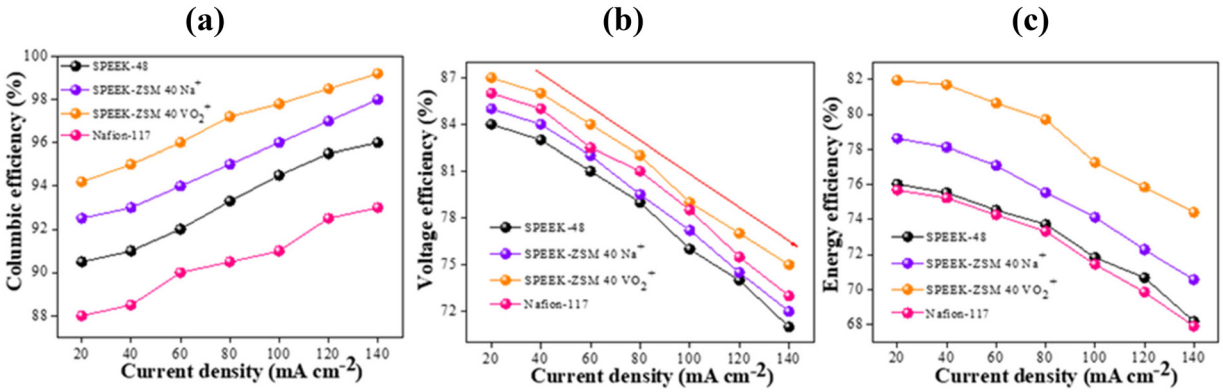

Fig. 9 Shows the rate performance of SPEEK-Zeolite composite membrane along with Nafion-117 Membranes: (a) coulombic efficiency, (b) voltage efficiency, (c) energy efficiency at 20 to 140 mA cm^{-2} current density.

SPEEK-ZSM 40 VO_2^+ membranes, consistent with their respective diffusion coefficient values. The high CE values observed for the SPEEK-ZSM 40 VO_2^+ membranes at current densities of 20, 40, 60, 80, 100, 120, and 140 mA cm^{-2} are 94.2%, 95%, 96%, 97.2%, 97.8%, 98.5%, and 99.2%, respectively. In contrast, the lower CE of the Nafion-117® membrane can be attributed to its well-defined, non-selective cation-conducting channels, which contribute to its reduced efficiency in ion selectivity. Nevertheless, these defined ion-conducting channels are absent in SPEEK-48 and the zeolite-filled membranes. Additionally, the presence of zeolite, without compromising ion selectivity, enhances ion transport across the membrane, resulting in higher CE values.[60]

Fig. 9(b) and (c) show the voltage efficiency (VE) and energy efficiency (EE) of the membranes. As expected, VE decreases with increasing current density due to the increase in ohmic resistance of the membranes.[61] The best-performing membrane, SPEEK-ZSM 40 VO_2^+, had VE values of 87%, 86%, 84%, 82%, 79%, 77%, and 75% at current densities ranging from 20 to 140 mA cm^{-2}. This data suggests that the addition of VO_2^+ exchanged zeolite enhances both selectivity and proton transport across the membrane. The energy efficiency (EE), which is the product of CE and VE, follows the same trend as VE. Correspondingly, the EE measured at these current densities was 81.90%, 81.70%, 80.60%, 79.70%, 77.20%, 75.80%, and 74.80%, respectively. The increased VE in VRFB is primarily due to the selective transport of protons over vanadium ions through the SPEEK-ZSM 40 VO_2^+ membrane. The engineered pore size of the zeolite allows smaller protons to pass while blocking larger vanadium ions, minimizing crossover. The shorter ion transport path the zeolite provides enhances proton conduction, further improving VE by maintaining a stable and efficient battery operation.

Following the rate performance evaluation, a long cycling test was conducted at a current density of 80 mA cm^{-2}. Fig. 10 shows the results of 200 galvanostatic charge/discharge cycles for SPEEK-48, SPEEK-ZSM 40 Na^+, SPEEK-ZSM 40 VO_2^+, and Nafion-117® membranes under identical experimental conditions. The data reveal that the SPEEK-ZSM 40 VO_2^+ membrane outperformed the others, with an impressive average CE of 97.94% and EE of 80.37% (Fig. 10(c)). The corresponding capacity retention was 54% over the first 100 charge–discharge cycles (ESI Fig. 4a†). Under the same experimental conditions, SPEEK-48, SPEEK-ZSM-40 Na^+, and Nafion-117® membranes exhibited CE values of 93.45%, 94.81%, and 90.89%, and EE values of 73.36%, 75.38%, and 72.90%, respectively (Fig. 10(a), (b), and (d)). The corresponding capacity retention (ESI Fig. 4a†) was 23%, 44%, and 13% for SPEEK-48, SPEEK-ZSM-40 Na^+, and Nafion-117® membranes over the first 100 charge–discharge cycles. Further, (ESI Fig. 4b†) illustrating capacity retention over time across 200 charge–discharge cycles demonstrates that the SPEEK-ZSM 40 VO_2^+ membrane exhibits outstanding cycling stability, sustaining a performance for ~1074 minutes. This surpasses the cycling durations of other membranes, including SPEEK-ZSM 40 Na^+ (827 min), SPEEK-48 (723 min), and Nafion-117® (673 min). These results highlight its superior stability and prolonged operational lifespan, which are vital for real-world applications in energy storage. Fig. 11(a), (b), (c), and (d) illustrates the overlapping charge–discharge curves for the 1st, 100th, and 200th cycles, demonstrating excellent capacity retention for the SPEEK-ZSM 40 VO_2^+ membrane. The superior performance of the SPEEK-ZSM 40 VO_2^+ membrane is attributed to the presence of VO_2^+ ions at the exchange proton sites of the zeolite.

Compared to the values in the literature, the CE and EE of this membrane were similar to the best-performing membranes reported. Fig. 12(a) and (b) present the CE and EE values of mixed-matrix membranes reported in the literature over the last decade, alongside those of the SPEEK-ZSM 40 VO_2^+ membrane. Yongsheng Xia *et al.* developed a molecularly cross-linked two-dimensional zeolite nanosheet (ZN) composite by incorporating ZN into a SPEEK matrix through acid–base interactions, achieving an exceptional CE of 99% and EE of 85% at a current density of 120 mA cm^{-2}.[27] Similarly, Jun Liu *et al.* synthesized a branched sulfonated polyimide (bSPI) composite membrane with sulfonated multi-wall carbon nanotubes (s-MWCNTs) as the filler, achieving a CE of 96% and EE of 79.7% at 80 mA cm^{-2}. The incorporation of s-MWCNTs

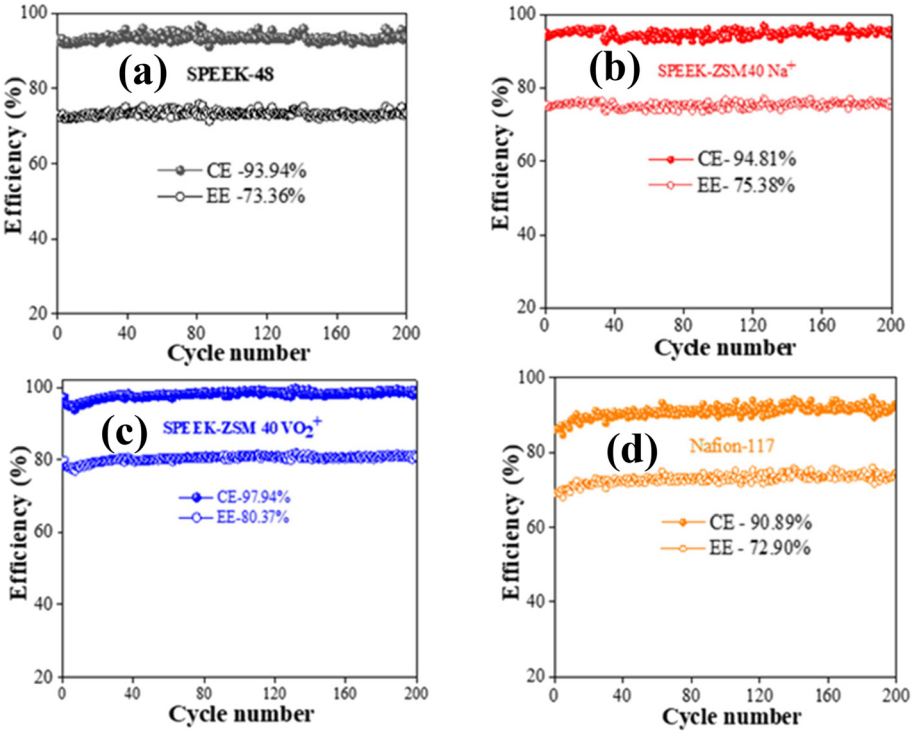

Fig. 10 Indicating CE and EE of the long charge–discharge 200 cycles (a), (b), (c) and (d) SPEEK, SPEEK-ZSM 40 Na^+, SPEEK-ZSM VO_2^+, and Nafion-117® respectively.

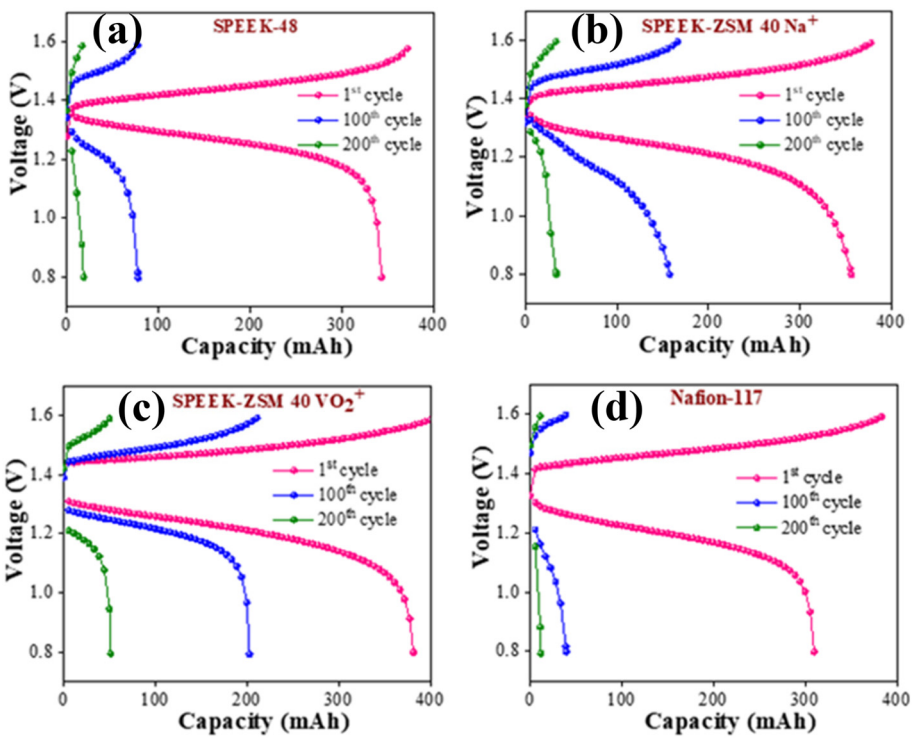

Fig. 11 The overlapping charge–discharge curves of the 1st, 100th, and 200th cycles for (a) SPEEK-48, (b) SPEEK-ZSM 40 Na^+, (c) SPEEK-ZSM 40 VO^{2+}, and (d) Nafion-117, respectively, at a current density of 80 mA cm^{-2}.

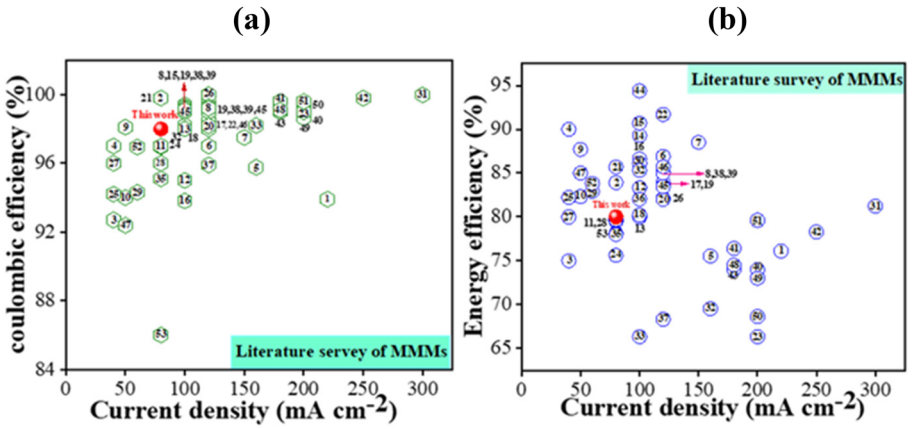

Fig. 12 (a) The coulombic efficiency (CE) and (b) the energy efficiency (EE) of membranes reported in the literature, along with the efficiency of the membrane presented in the current study. The red ball highlights the data point from the present study.

enhances proton-conducting channels while effectively restricting vanadium ion crossover through acid–base interactions, contributing to superior membrane performance.[62] Afzal *et al.* demonstrated that oxidized black phosphorus nanosheets (O-bPn) significantly enhance the ion selectivity of SPEEK membranes in VRFB. Incorporating 1.5% O-bPn into SPEEK (S/O-bPn-1.5%) achieved CE of 98.3% and EE of 86.6% at 100 mA cm^{-2}. The 2D puckered lattice of O-bPn forms proton-conductive channels, optimizing proton transport while reducing vanadium ion crossover. This organic–inorganic interaction enhances membrane performance.[63] To restrict the excess diffusion in the Nafion membrane Md. Abdul *et al.* incorporated $TiZrO_4$NT as an inorganic filler into the Nafion matrix, creating a tortuous pathway to block vanadium ion crossover, achieving an impressive CE of 99.8% and EE of 83.9% at 80 mA cm^{-2}.[64] This study underscores the importance of inorganic fillers like $TiZrO_4$NT in enhancing hydrophilicity and proton conductivity, leading to significant performance gains in VRFB applications. A related study reported the fabrication of a Nafion-neodymium zirconium oxide nanotube (Nafion-NdZr) composite membrane, specifically Nafion-NdZr (1%)/$[P\text{-}S]_2$, which achieved a CE of 92.7% and EE of 75% at 40 mA cm^{-2}. In this case, the $Nd_2Zr_2O_7$ nanotubes act as proton conductors while blocking vanadium ions, with an additional PDDA layer further enhancing vanadium ion selectivity.[65] Together, these studies highlight the critical role of nanofillers in reducing vanadium ion crossover, improving proton conduction, and optimizing the energy efficiency of VRFB membranes. These results underscore the enhanced performance of the SPEEK-ZSM-40 VO_2^+ membrane, demonstrating superior coulombic efficiency and capacity retention. The membrane's effectiveness is attributed to its utilization of the Donnan exclusion principle and proton selectivity, which collectively minimize ion crossover. Thus, the SPEEK-ZSM-40 VO_2^+ membrane shows significant potential for improving VRFB performance, representing a promising advancement in membrane technology for VRFB applications.

4. Conclusion

Vanadium ions (VO_2^+) were successfully incorporated into ZSM-5 zeolite through an ion-exchange method, resulting in vanadium-encased zeolite samples that retained their structural integrity, as confirmed by XRD and XPS analyses. The composite membranes with SPEEK exhibited good oxidative stability in a 2 M H_2SO_4 solution containing 1.5 M VO_2^+ ions, owing to the combined effects of Donnan exclusion and ion sieving by the zeolite, which effectively minimized vanadium crossover. Electrochemical and physicochemical properties evaluations showed that the MMMs outperformed pristine SPEEK-48 membranes, demonstrating superior proton conductivity and enhanced stability in acidic electrolytes. In a VRFB tests, the membrane with excellent vanadium ion selectivity, SPEEK-ZSM-40 VO_2^+, surpassed both Nafion-117 and SPEEK-48 membranes, achieving a CE of ~98.0% and an EE of 80.37% at a current density of 80 mA cm^{-2} over 200 continuous charge–discharge cycles. Moreover, it retained 54% of its capacity after 100 cycles. Polarization curve analysis and self-discharge experiments, revealed a significantly higher peak power density of 330.45 mW cm^{-2} and a 1.3-fold slower self-discharge rate compared to Nafion-117®, underscoring the membrane's enhanced operational efficiency. These findings highlight the potential of vanadium-encased zeolites within a SPEEK framework, leveraging both Donnan exclusion and size-exclusion principles to create efficient and durable membranes. This approach offers substantial advantages for VRFB applications and presents a promising alternative for developing metal ion-selective membranes in energy storage devices.

Data availability

The data supporting this article have been included as part of the ESI.†

Conflicts of interest

There are no conflicts to declare.

Acknowledgements

The authors acknowledge the Director of CSIR-CSMCRI for continuous support and encouragement. R. K. N. acknowledges the financial support from Council for Science and Industrial Research, India (Project No. NCP060305). The instrumentation facilities provided by the Analytical Discipline & Centralized Instrument Facility, CSIR-CSMCRI, Bhavnagar, are gratefully acknowledged. This is CSIR-CSMCRI manuscript number–.

References

1 A. Z. Weber, M. M. Mench, J. P. Meyers, P. N. Ross, J. T. Gostick and Q. Liu, Redox flow batteries: a review, *J. Appl. Electrochem.*, 2011, **41**, 1137–1164.
2 N. Zhao, A. Platt, H. Riley, R. Qiao, R. Neagu and Z. Shi, Strategy towards high ion selectivity membranes for all-vanadium redox flow batteries, *J. Energy Storage*, 2023, **72**, 108321.
3 H. Prifti, A. Parasuraman, S. Winardi, T. M. Lim and M. Skyllas-Kazacos, Membranes for Redox Flow Battery Applications, *Membranes*, 2012, **2**(2), 275–306.
4 S. Sreenath, C. M. Pawar, P. Bavdane, D. Y. Nikumbe and R. K. Nagarale, A sulfonated polyethylene–styrene cation exchange membrane: a potential separator material in vanadium redox flow battery applications, *Energy Adv.*, 2022, **1**, 87.
5 B. Jiang, L. Wu, L. Yu, X. Qiu and J. Xi, A comparative study of Nafion series membranes for vanadium redox flow batteries, *J. Membr. Sci.*, 2016, **510**, 18–26.
6 J. S. Lawton, A. M. Jones, Z. Tang, M. Lindsey and T. Zawodzinski, Ion Effects on Vanadium Transport in Nafion Membranes for Vanadium Redox Flow Batteries, *J. Electrochem. Soc.*, 2017, **164**, 13.
7 C. H. Lin, M. C. Yang and H. J. Wei, Amino-silica modified Nafion membrane for vanadium redox flow battery, *J. Power Sources*, 2015, **282**, 562–571.
8 J. Xi, W. Daia and L. Yu, Polydopamine coated SPEEK membrane for a vanadium redox flow battery, *RSC Adv.*, 2015, **5**, 33400.
9 D. Zhang, L. Xin, Y. Xia, L. Dai, K. Qu, K. Huang, Y. Fan and X. Zhi, Advanced Nafion hybrid membranes with fast proton transport channels toward high-performance vanadium redox flow battery, *J. Membr. Sci.*, 2021, **624**, 119047.
10 Y. Shia, C. Eze, B. Xiong, W. He, H. Zhang, T. M. Lim, A. Ukil and J. Zhao, Recent development of membrane for vanadium redox flow battery applications: A review, *Appl. Energy*, 2019, **238**, 202–224.
11 D. Düerkop, H. Widdecke, C. Schilde, U. Kunz and A. Schmiemann, Polymer membranes for all-vanadium redox flow batteries: a review, *Membranes*, 2021, **11**, 214.
12 J. Li, F. Xu, W. Chen, Y. Han and B. Lin, Anion exchange membranes based on bis-imidazolium and imidazolium-functionalized poly(phenylene oxide) for vanadium redox flow battery applications, *ACS Omega*, 2023, **8**, 16506–16512.
13 S. Sreenath, P. S. Nayanthara, C. M. Pawar, D. Y. Nikumbe, B. Bhatt, J. C. Chaudhari and R. K. Nagarale, High-Capacity Retention Thermally Reinforced Pore-Filled Anion Exchange Membrane for All-Vanadium Flow Batteries, *ACS Appl. Energy Mater.*, 2022, **5**, 13661–13671.
14 P. S. Nayanthara, S. Sreenath, A. Ash, C. M. Pawar, V. Dave, V. Verma and R. K. Nagarale, Robust Polyaniline-silica@polypropylene for High-Performance, High-Capacity Retention All-Vanadium Redox Flow Battery, *ACS Appl. Energy Mater.*, 2024, **7**, 2338–2350.
15 N. Shi, G. Wang, Q. Wang, L. Wang, Q. Li and J. Yang, Acid doped branched poly (biphenyl pyridine) membranes for high-temperature proton exchange membrane fuel cells and vanadium redox flow batteries, *Chem. Eng. J.*, 2024, **489**, 151121.
16 J. Yang, P. Lv, W. Tang and Q. Wang, Sulfonate and Ammonium-Grafted Poly (isatin triphenyl) Membranes for the Vanadium Redox Flow Battery, *ACS Appl. Polym. Mater.*, 2024, **6**, 10727–10737.
17 S. J. Seo, B. C. Kim, K. W. Sung, J. Shim, J. D. Jeon, K. H. Shin, S. H. Shin, S. H. Yun, J. Y. Lee and S. H. Moon, Electrochemical properties of pore-filled anion exchange membranes and their ionic transport phenomena for vanadium redox flow battery applications, *J. Membr. Sci.*, 2013, **428**, 17–23.
18 P. Qian, W. Zhou, Y. Zhang, D. Chao and M. Song, Review and Perspectives of Sulfonated Poly(ether ether ketone) Proton Exchange Membrane for Vanadium Flow Batteries, *Energy Fuels*, 2023, **37**, 17681–17707.
19 S. M. Park, S. H. Lee and H. Kim, Fabrication and Characterization of Composite Membranes for Vanadium Redox Flow Batteries, *ECS Meet. Abstr.*, 2016, **230**, 4018–4018.
20 J. Ye, C. Wu, W. Qin, F. Zhong and M. Ding, Advanced Sulfonated Poly(Ether Ether Ketone)/Graphene-Oxide/Titanium Dioxide Nanoparticle Composited Membrane with Superior Cyclability for Vanadium Redox Flow Battery, *J. Nanosci. Nanotechnol.*, 2020, **20**, 4714–4721.
21 K. Brahma, R. Nayak, S. K. Verma and Sonika, Recent advances in development and application of polymer nanocomposite ion exchange membrane for high performance vanadium redox flow battery, *J. Energy Storage*, 2024, **97**, 112850.
22 P. Qian, W. Zhou, Y. Zhang, D. Chao and M. Song, Review and Perspectives of Sulfonated Poly(ether ether ketone) Proton Exchange Membrane for Vanadium Flow Batteries, *Energy Fuels*, 2023, **37**, 17681–17707.
23 B. G. Thiamz and S. Vaudreuil, Review—Recent Membranes for Vanadium Redox Flow Batteries, *J. Electrochem. Soc.*, 2021, **168**, 070553.

24 Y. Jiaye, X. Lu, L. Huiyun, F. P. G. d. Arquer and H. Wang, The Critical Analysis of Membranes toward Sustainable and Efficient Vanadium Redox Flow Batteries, *Adv. Mater.*, 2024, **36**, 2402090.

25 X. Shi, O. C. Esan, X. Huo, Y. Ma, Z. Pan, L. An and T. S. Zhao, Polymer Electrolyte Membranes for Vanadium Redox Flow Batteries: Fundamentals and Applications, *Prog. Energy Combust. Sci.*, 2021, **85**, 100926.

26 Y. Xia, H. Cao, F. Xu, Y. Chen, Y. Xia, D. Zhang, L. Dai, K. Qu, C. Lian, K. Huang, W. Xing, W. Jin and Z. Xu, Polymeric membranes with aligned zeolite nanosheets for sustainable energy storage, *Nat. Sustainability*, 2022, **5**, 1080–1091.

27 Y. Xia, Y. Wang, L. Xiao, Y. Yu, J. Ji, Y. Xi, K. Qu, K. Huang, W. Xing and Z. Xu, Functional molecular cross-linked zeolite nanosheets heighten ion selectivity and conductivity of flow battery membrane, *AIChE J.*, 2023, **69**(4), 17964.

28 Y. Cai, S. Lin, Y. Xia, Q. Hou, Y. Lu, H. Cao, Y. Wang, K. Huang and Z. Xu, ZSM-5 zeolite incorporated flow battery membranes with regulated pore channels for high proton conduction, *AIChE J.*, 2024, **70**, 18380.

29 R. Yang, Z. Cao, S. Yang, I. Michos, Z. Xu and J. Dong, Colloidal silicalite-nafion composite ion exchange membrane for vanadium redox-flow battery, *J. Membr. Sci.*, 2015, **484**, 1–9.

30 C. M. Pawar, S. Sreenath, B. Bhatt, V. Dave, P. S. Nayanthara, W. F. G. Saleha, G. Sethia and R. K. Nagarale, Proton conducting zeolite composite membrane boosts the performance of vanadium redox flow battery, *Solid State Ionics*, 2024, **404**, 116417.

31 D. Palamara, P. Bruzzaniti, L. Calabrese and E. Proverbio, Effect of degree of sulfonation on the performance of adsorbent SAPO-34/S-PEEK composite coatings for adsorption heat pumps, *Prog. Org. Coat.*, 2021, **154**, 106193.

32 C. M. Pawar, S. Sreenath, V. Dave, P. P. Bavdane, V. Singh, V. Verma and R. K. Nagarale, Chemically stable and high acid recovery anion exchange membrane, *Polymer*, 2022, **251**, 124915.

33 P. P. Bavdane, S. Sreenath, D. Y. Nikumbe, C. M. Pawar, M. C. Kuzhiyil and R. K. Nagarale, N-Sulfonated Poly (arylene-oxindole) for Vanadium Redox Flow Battery Applications, *ACS Appl. Energy Mater.*, 2022, **5**(11), 13189–13199.

34 P. P. Bavdane, S. Sreenath, D. Y. Nikumbe, B. Bhatt, C. M. Pawar, V. Dave and R. K. Nagarale, A poly(2-ethylaniline) blend membrane for vanadium redox flow batteries, *RSC Appl. Polym.*, 2024, **2**, 87–97.

35 L. Cao, A. Kronander, A. Tang, D. W. Wang and M. S. Kazacos, Membrane Permeability Rates of Vanadium Ions and Their Effects on Temperature Variation in Vanadium Redox Batteries, *Energies*, 2016, **9**, 1058.

36 P. Wang, X. Xiao, Y. Pan, Z. Zhao, G. Jiang, Z. Zhang, F. Meng, Y. Li, X. Fan, L. Kong and Z. Xie, Facile Synthesis of Nanosheet-Stacked Hierarchical ZSM-5 Zeolite for Efficient Catalytic Cracking of n-Octane to Produce Light Olefins, *Catalysts*, 2022, **12**, 351.

37 S. Lai, D. Meng, W. Zhan, Y. Guo, Y. Guo, Z. Zhang and G. Lu, The promotional role of Ce in Cu/ZSM-5 and in situ surface reaction for selective catalytic reduction of NOx with NH_3, *RSC Adv.*, 2015, **5**, 90235.

38 Q. Zou, M. Liu, M. Fan, Y. Ding, Y. Chen and S. Shen, Effect of Na+ on catalytic performance of CoCe/ZSM-5 catalysts for oxidation of toluene, *J. Rare Earths*, 2021, **39**, 409–418.

39 W. Rongchapo, C. Keawkumay, N. Osakoo, K. Deekamwong, N. Chanlek, S. Prayoonpokarach and J. Wittayakun, Comprehension of paraquat adsorption on faujasite zeolite X and Y in sodium form, *Adsorpt. Sci. Technol.*, 2017, (0), 1–10.

40 G. Silversmit, D. Depla, H. Poelman, G. B. Marin and R. D. Gryse, Determination of the V2p XPS binding energies for different vanadium oxidation states (V5+ to V0+), *J. Electron Spectros, Relat. Phenomena*, 2004, **135**, 167–175.

41 S. Senthilkumar, W. Zhong, M. Natarajan, C. Lu, B. Xu and X. Liu, A green approach for aerobic oxidation of benzylic alcohols catalyzed by CuI–Y zeolite/TEMPO in ethanol without additional additives, *New J. Chem.*, 2021, **45**, 705.

42 H. T. T. Nguyen, D. Jung, C. Y. Park and D. J. Kang, Synthesis of single-crystalline sodium vanadate nanowires based on chemical solution deposition method, *Mater. Chem. Phys.*, 2015, **165**, 19–24.

43 X. Liu, S. Gao, F. Yang, S. Zhou and Y. Kong, High promoting of selective oxidation of ethylbenzene by Mn ZSM 5 synthesized without organic template and calcination, *Res. Chem. Intermed.*, 2020, **46**, 2817–2832.

44 Z. Jiang, D. Chen, W. Deng and L. Guo, Different morphological ZSM-5 zeolites supported Pt catalysts for toluene catalytic combustion, *Chem. Phys. Impact*, 2022, **5**, 100134.

45 Q. L. Wang, G. Giannetto, M. Torrealba, G. Perot, C. Kappenstein and M. Guisnet, Dealumination of Zeolites1 II. Kinetic Study of the Dealumination by Hydrothermal Treatment of a NH4NaY Zeolite, *J. Catal.*, 1991, **130**, 459–470.

46 K. V. Cruz, A. Lam and C. M. Z. Wilson, Full Mechanism of Zeolite Dealumination in Aqueous Strong Acid Medium: Ab Initio Periodic Study on H-Clinoptilolite, *J. Phys. Chem. C*, 2017, **121**, 2652–2660.

47 Y. Wang, Y. Zhou, X. Zhang, Y. Gao and J. Li, SPEEK membranes by incorporation of NaY zeolite for CO2/N2 separation, *Sep. Purif. Technol.*, 2021, **275**, 119189.

48 E. C. Tzi and O. P. Ching, Surface modification of AMH-3 for the development of mixed matrix membranes, *Procedia Eng.*, 2016, **148**, 86–92.

49 Z. Li, W. Dai, L. Yu, J. Xi, X. Qiu and L. Chen, Sulfonated poly(ether ether ketone)/mesoporous silica hybrid membrane for high-performance vanadium redox flow battery, *J. Power Sources*, 2014, **257**, 221–229.

50 M. Taha, L. H. M. Edwin, M. R. Field, M. Sun, M. Singhd and W. Zou, Room-temperature application of VO2 microstructures on rigid and flexible substrates based on synthesis of crystalline VO2 solution, *Mater. Adv.*, 2020, **1**, 1685.

51 J. I. Contreras-Rascón, J. Díaz-Reyes, A. Flores-Pacheco, R. L. Morales, M. E. Álvarez-Ramos and J. A. Balderas-López, Structural and optical modifications of CdS properties in CdS-Au thin films prepared by CBD, *Results Phys.*, 2021, **22**, 103914.
52 R. K. Gogoi, A. B. Neog, T. J. Konch, N. Sarmah and K. Raidongia, A two-dimensional ion-pump of a vanadium pentoxide nanofluidic membrane, *J. Mater. Chem. A*, 2019, **7**, 10552.
53 H. M. Ibrahim and A. G. Alghamdi, Effect of the Particle Size of Clinoptilolite Zeolite on Water Content and Soil Water Storage in a Loamy Sand Soil, *Water*, 2021, **13**(5), 607.
54 Z. Xu, I. Michos, Z. Cao, W. Jing, X. Gu, K. Hinkle, S. Murad and J. Dong, Proton-Selective Ion Transport in ZSM-5 Zeolite Membrane, *J. Phys. Chem. C*, 2016, **120**, 26386–26392.
55 H. Cho, H. M. Krieg and J. A. Kerres, Application of Novel Anion-Exchange Blend Membranes (AEBMs) to Vanadium Redox Flow Batteries, *Membranes*, 2018, **8**, 33.
56 C. M. Pawar, S. Sreenath, B. Bhatt, D. Y. Nikumbe, W. F. G. Saleha and R. K. Nagarale, Surface modification, counter-ion exchange effect on thermally annealed sulfonated poly (ether ether ketone) membranes for vanadium redox flow battery, *Colloids Surf., A*, 2023, **667**, 131295.
57 C. Ding, H. Zhang, X. Li, T. Liu and F. Xing, Vanadium flow battery for energy storage: prospects and challenges, *J. Phys. Chem. Lett.*, 2013, **4**, 1281–1294.
58 D. Chen, M. A. Hickner, E. Agar and E. C. Kumbur, Optimized Anion Exchange Membranes for Vanadium Redox Flow Batteries, *ACS Appl. Mater. Interfaces*, 2013, **5**(15), 7559–7566.
59 R. Yang, Z. Xu, S. Yang, I. Michos, L. F. Li, A. P. Angelopoulos and J. Dong, Nonionic zeolite membrane as potential ion separator in redox-flow battery, *J. Membr. Sci.*, 2014, **450**, 12–17.
60 C. Jia, J. Liu; and C. Yan, A significantly improved membrane for vanadium redox flow battery, *J. Power Sources*, 2010, **195**, 4380–4383.
61 J. C. Duburg, B. Chen, S. Holdcroft, T. J. Schmidt and L. Gubler, Design of polybenzimidazole membranes for use in vanadium redox flow batteries, *J. Mater. Chem. A*, 2024, **12**, 6387.
62 J. Liu, H. Duan, W. Xu, J. Long, W. Huang, H. Luo, J. Li and Y. Zhang, Branched sulfonated polyimide/s-MWCNTs composite membranes for vanadium redox flow battery application, *Int. J. Hydrogen Energy*, 2021, **46**, 34767–34776.
63 Afzal, W. Chen, B. Pang, X. Yan, X. Jiang, F. Cui, X. Wu and G. He, Oxidized black phosphorus nanosheets/sulfonated poly (ether ether ketone) composite membrane for vanadium redox flow battery, *J. Membr. Sci.*, 2022, **644**, 120084.
64 M. Abdul Aziz, D. Han and D. S. Shanmugam, Ultrahigh proton/vanadium selective and durable Nafion/$TiZrO_4$ composite membrane for high-performance all-vanadium redox flow batteries, *ACS Sustainable Chem. Eng.*, 2021, **9**, 11041–11051.
65 S. I. Hossain, M. A. Aziz and S. Shanmugam, Ultrahigh ion-selective and durable Nafion-NdZr composite layer membranes for all-vanadium redox flow batteries, *ACS Sustainable Chem. Eng.*, 2020, **8**, 1998–2007.